corresponds to a DCF of 16.5 ± 4.7% (2σ), similar to the range typically found for speleothems of 16 ± 5% (*34*, *35*). In spite of the strong resemblance between the GB-89-24-1 and INTCAL98 records suggesting nearly constant DCF, there are two moderate departures, which may be due to chronological errors in either GB-89-24-1 or INTCAL98 or, alternatively, to fluctuations in DCF. We are currently unable to resolve between these possibilities, although GB-89-24-1 is in better agreement with the Lake Suigetsu data (*13*) (Fig. 2) and the newly revised Cariaco Basin record (*12*), suggesting that revisions to INTCAL98 may be merited. Nevertheless, because of the uncertain origin of these two departures, we incorporate a conservative estimate of DCF uncertainty of 4.7% (2σ) in the overall precision of DCF-corrected ^{14}C age and $\Delta^{14}C$. This value is used, rather than $2\sigma_m$, because we acknowledge the possibility of residual structure in the ^{14}C age offset because of chronological differences, minor DCF variation, or differences in expected amplitude of variation between GB-89-24-1 and INTCAL98, which is based on the dampened signal of the mixed layer of the ocean. With this conservative error estimate, the relative contribution of uncertainty in DCF to the overall $\Delta^{14}C$ error diminishes with increasing calendar age from ~50% at 11 ka to ~10% at 45 ka.

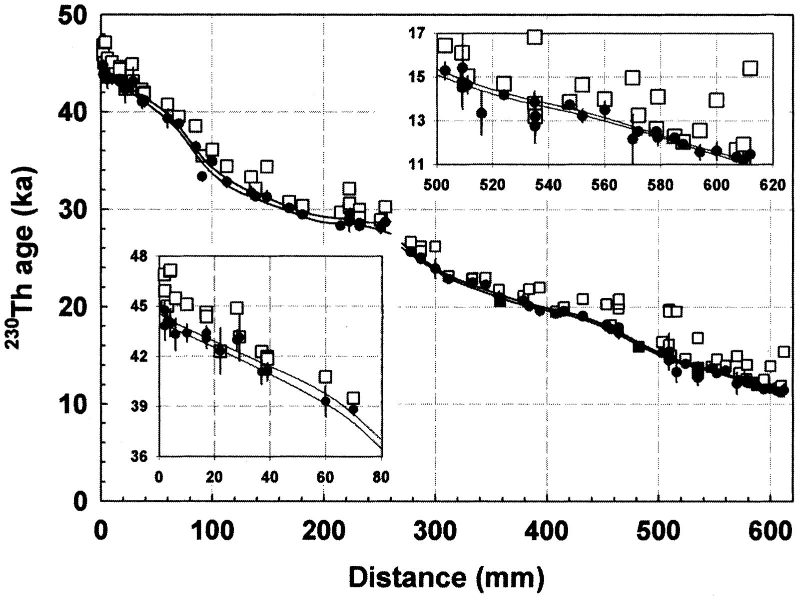

Fig. 1. ^{230}Th age versus distance along the longitudinal growth axis of GB-89-24-1, a submerged speleothem from −14.4 m in Sagittarius, Zodiac Caverns, Grand Bahama. ^{230}Th age is corrected for initial Th with $^{230}Th/^{232}Th_{init}$ activity ratio with a bulk Earth value of 0.8 ± 0.8 parts per million (□) and a substantially higher value of 18.7 ± 2.9 based on isochron results (●). The latter correction provides a smoother, monotonic distance-age relation. Confidence bands (95%) of a weighted smoothing spline with a roughness penalty approach (*30*) are plotted for each of the phases of growth before and after shift in drip locus between ~28 and 26 ka. These curves are used to predict calendar age and error for each of the subsamples selected for AMS ^{14}C analysis. Inset figures show expanded views of the oldest (bottom inset) and youngest (top inset) parts of the record.

Fig. 2. Radiocarbon age versus calendar age for GB-89-24-1, Lake Suigetsu laminated sediments (*13*), and the INTCAL98 spline (*1*) for the period 15.5 to 11 ka. All ages are plotted with 2σ errors, except the INTCAL98 spline fit (1σ). Radiocarbon ages for GB-89-24-1 are not corrected for DCF; calendar ages and errors are based on the predicted longitudinal growth–^{230}Th age model with the spline fit illustrated in Fig. 1. Each set of data—speleothem, marine tree-ring compilation, and lake varves—shows a similar general pattern. The offset between INTCAL98 and GB-89-24-1 is relatively constant, with a mean value of 1450 ± 470 years (2σ) during a period of marked climate change. The constant offset is attributed to a relatively stable DCF of 16.5 ± 4.7 (2σ).

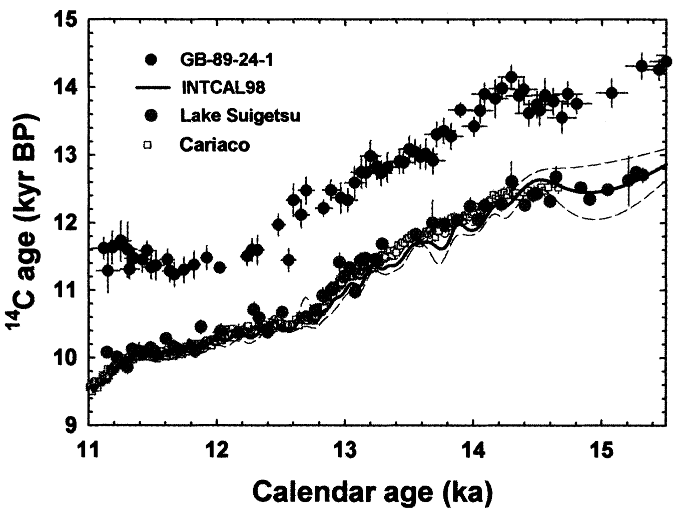

DCF-corrected ^{14}C ages for GB-89-24-1 show good agreement with other records between 11 and 26 ka (Fig. 3A), although before 30 ka, none of these records are in accord with each other. Between 30 and 45 ka, the Lake Suigetsu (*13*), Icelandic Sea (*14*), and Lake Lisan (*8*) records all exhibit generally older radiocarbon ages (or younger calendar ages) than GB-89-24-1. The Cango Cave record (*19*) is in general agreement with GB-89-24-1 although the data are sparse and its uncertainties are large. The available coral data (*4*, *7*) are in substantial agreement with GB-89-24-1 before 30 ka but reveal a high degree of scatter at older ages. One possible source of disagreement between GB-89-24-1 and other records between 30 and 45 ka could be fluctuations in DCF. We note, however, that large DCF fluctuations were not observed in GB-89-24-1 during the deglacial period, a period of marked climate change when DCF variability would be expected to be at a maximum. Furthermore, even if we were to allow DCF to go to its theoretical limit (i.e., no dead carbon), it still would not be possible to adjust GB-89-24-1 to match either the Icelandic Sea, Lake Suigetsu, or Lake Lisan records between 30 and 45 ka. We therefore assert that this discordance is largely due to other sources. Other possible sources of discordance between these records include incorrect initial ^{230}Th correction to ^{230}Th ages, unsupported gain or loss of U or Th, missing or uncounted varves in the Lake Suigetsu chronology, or, in the case of the Icelandic Sea record, uncertainty in the marine reservoir correction, errors in matching the ocean sediment $\delta^{18}O$ record to the Greenland Ice Sheet Project 2 (GISP2) $\delta^{18}O$ record, or uncertainties in the GISP2 chronology itself (*36*). We note parenthetically here that the Icelandic Sea record exhibits very similar structure to GB-89-24-1 and that an arbitrary 2-ka phase shift in calendar age before 25 ka brings these records into substantial agreement. This observation suggests that a discrepancy in calendar age may be the chief cause of disagreement between these two records.

The record of past atmospheric $\Delta^{14}C$ concentration derived from GB-89-24-1 (Fig. 3B) shows a broad maxima occurring between 44.5 and 33 ka, which can be divided into a relatively short but intense excursion occurring between 44.3 and 43.3 ka and a much longer set of peaks between 42 and 33 ka B.P. The magnitude of the initial excursion is enormous, with the maximum values reaching ~1300 per mil (‰) (for the fitted spline), which is nearly twice as high as the "bomb-pulse" spike resulting from atmospheric nuclear weapons testing during the 1950s and 1960s. The other main features of this record are a marked drop in $\Delta^{14}C$ occurring between 35 and 33 ka, followed by a general 40% decline occurring between 26 and 11 ka. Smaller millennial-scale oscillations are superimposed on this latter decline, although some of these smaller oscillations may not be distinguishable from fluctuations caused by variations in DCF. Although it is possible that part of the largest excursions in $\Delta^{14}C$ excursion could be due to changes in DCF, we again note that even if DCF was reduced to the theoretical zero value, this 16.5% shift in DCF will only reduce these excursions by a small fraction. Thus, it is clear that the main cause of these large $\Delta^{14}C$ excursions is something other than fluctuations in DCF.

^{14}C modeling results. Enhancements in cosmogenic ^{36}Cl and ^{10}Be isotope concentrations at circa 30 to 45 ka have previously been observed in polar ice cores (*37–39*) and marine sediments (*40*), suggesting that atmospheric $\Delta^{14}C$ should also be elevated during this time frame. It has been known for some time that glacial age atmospheric ^{14}C levels were higher and more variable than during the Holocene (*16*, *17*, *41*), but the magnitude of variation revealed by our stalagmite record is nevertheless surprising. There are four main factors that can influence atmospheric ^{14}C concentration: primary cosmic ray flux, strength of the solar electromagnetic field, terrestrial magnetic field intensity, and the structure of the carbon cycle (*42–45*).
these factors control th
production rate, wherea
controls the distribution
various carbon reservoir
galactic cosmic rays ((
most terrestrial ^{14}C pr
solar cosmic rays can
percent of total producti
riods of unusually ene
events (*42*, *46*). Althoug
flux or energy spectra
source of the observed
spheric $\Delta^{14}C$, it is ge
have remained fairly c
very long time scales (
Electromagnetic fields a
Sun and solar wind and t
netic field intensity both modulate atmospheric ^{14}C production by attenuating the amount of GCR reaching Earth's atmosphere through a number of scattering mechanisms (*47*, *48*). These solar effects are modulated on the 11-year sunspot cycle (*49*, *50*) as well as several other longer cycles (*51*, *52*), which can produce about a factor of two variation in atmospheric ^{14}C production (*53*), with more production occurring during periods of low solar activity. For the normal range in cosmic ray energies incident on Earth's atmosphere, the globally integrated ^{14}C production rate also varies approximately in proportion to the inverse square root of Earth's magnetic field intensity [except at low geomagnetic field intensity where this relation diverges (*42*, *43*)]. At least a twofold variability in global ^{14}C production rate can be explained by the range of dipole magnetic field intensities during the past 50 ka (*42*, *43*).

To isolate which of these factors is responsible for the large observed variations in atmospheric $\Delta^{14}C$ for the period 45 to 11 ka, we performed several model simulations in which ^{14}C production regulation mechanisms were varied. For each simulation, a particular carbon cycle was specified because this substantially influences the distribution of ^{14}C between the various carbon reservoirs. We first chose the simplest case of an invariant balanced modern carbon cycle (*54*). Reservoir sizes and fluxes were brought to an initial balanced state in which both ^{12}C and

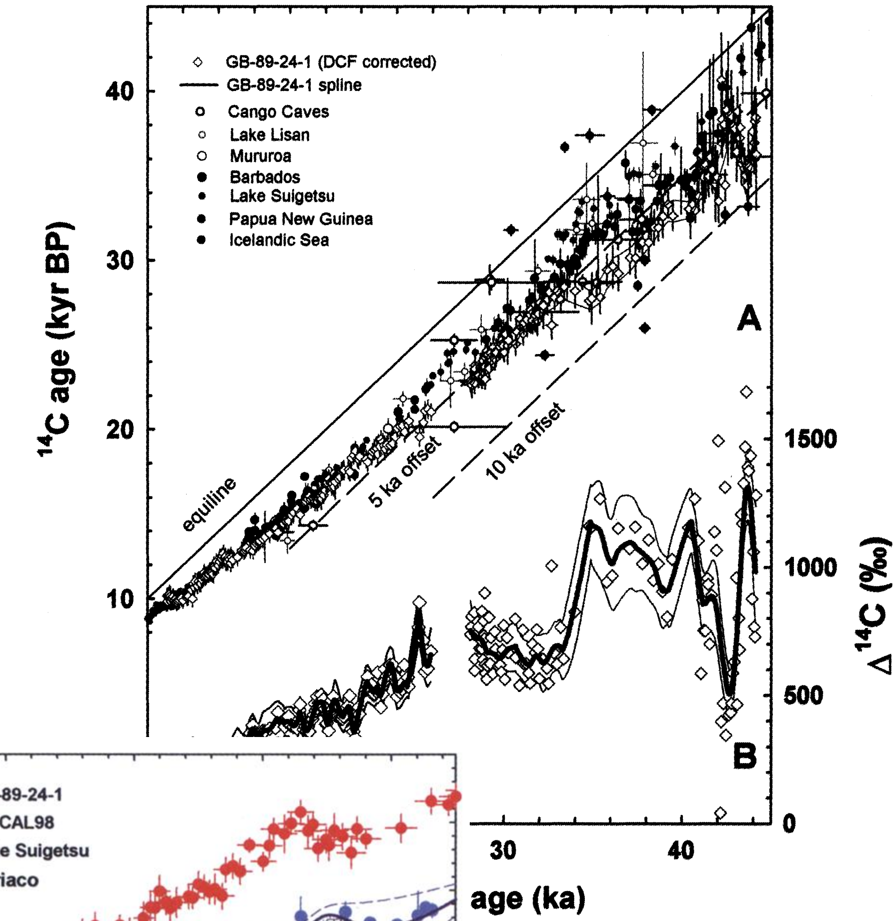

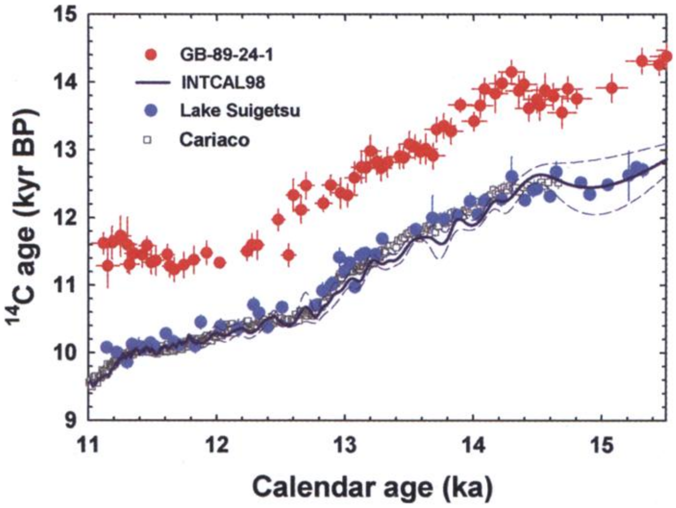

ons in atmospheric $\Delta^{14}C$ based on GB-89-24-1
^{14}C records. (**A**) DCF-corrected ^{14}C age versus
talagmite GB-89-24-1. Error bars for GB89-24-1
easurement precision, ^{14}C chemical blank, DCF
are 2σ for all other data, except for Cango Caves
term for both ^{14}C measurement precision and
ta (*14*), where zero uncertainty was assumed for
ifera data are corrected with a marine reservoir
it back to ~32 ka but exhibit substantial scatter
the GB-89-24-1 ^{14}C time scale between 45 and
; both raw data and smoothed spline with 95%
eak of about 1 ka in duration is observed in
out 1300‰—nearly twice as high as the 20th-century bomb pulse. Another broader $\Delta^{14}C$ maximum is observed between 42 and 33 ky B.P. This maxima appears to coincide broadly with the geomagnetic intensity minimum expressed in the SINT200 stacked geomagnetic record (*57*). Both peaks occur at about the same time as peaks of cosmogenic isotopes ^{10}Be and ^{36}Cl found in the Greenland Ice Sheet Project polar ice core (*38*, *39*).

^{14}C concentrations reflected the modern pre-bomb abundances (*45*, *55*, *56*). All model runs were initialized at 72 ka to eliminate any initial state transient behavior before entering the time window of interest (50 to 10 ka). In the first model run, we simulated the effects of geomagnetic modulation alone on ^{14}C production using the SINT-200 stacked paleomagnetic record (*57*). Results from this first model run matched the modern ^{14}C abundance for all carbon reservoirs after the 72-ka run time, and we obtained a long-term trend similar to that of Bard (*16*). This simulation, however, obtained peak levels of atmospheric $\Delta^{14}C$ that were about 700‰ lower than those observed in our stalagmite record for the magnetic field minima conditions between 40 and 35 ka and about 1000‰ lower than the peak values observed at the ~44-ka peak (Fig. 4A). In addition, the gradient of $\Delta^{14}C$ variations younger than 30 ka is much lower than that observed in GB-89-24-1 and other records. Thus, geomagnetic modulation alone cannot explain the variability in $\Delta^{14}C$ observed in GB-89-24-1. Simulation of a reduction of solar modulation to very low levels was also found to be insufficient to produce the GB-89-24-1 atmospheric $\Delta^{14}C$ record. Using the same carbon cycle model, and dropping solar electromagnetic modulation of GCR to zero for the length of the 44.3- to 43.3-ka excursion produces a $\Delta^{14}C$ excursion no greater than 150 to 200‰, which is only about one-fifth as large as required.

New paleomagnetic evidence from North Atlantic sediment cores (*58*, *59*) suggests that geomagnetic field intensity may have dropped to much lower strength during the

inclination excursion, the magnetic field inclination may have rotated by as much as 180° with field intensity dropping to less than 10% of modern levels. The age of this excursion is controversial but is thought to be somewhere between 33 and 45 ka in age. Because the timing and duration of the Laschamp inclination excursion are similar to those of the ~44-ka ^{14}C excursion observed in our stalagmite record, it is plausible that the Laschamp excursion was coincident with this ^{14}C excursion. Nevertheless, our model simulations show that reducing both the solar and terrestrial magnetic fields to their theoretical limits of zero between 44.5 and 43.8 ka still produces only ~50% of the observed excursion amplitude and does not produce the

ob-
sing
om-
ula-
eral
our
that
ged
that
ust
, or

ally
on
me
Mc-
^{10}Be
for-
^{10}Be
ical
geo-
hey
and
ova
uld
ield
ob-
Al-
44-
4-1,
ase
tely
lern

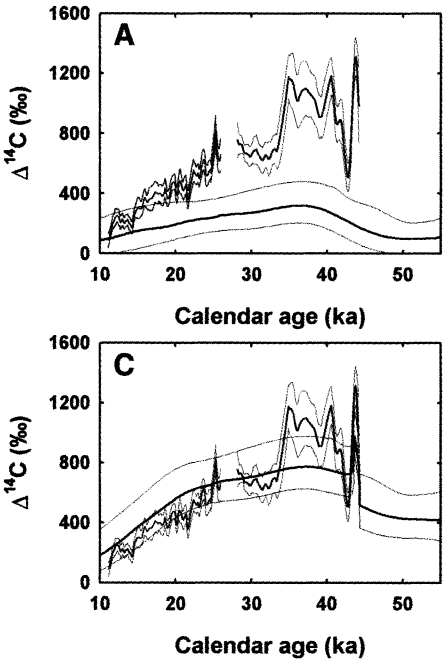

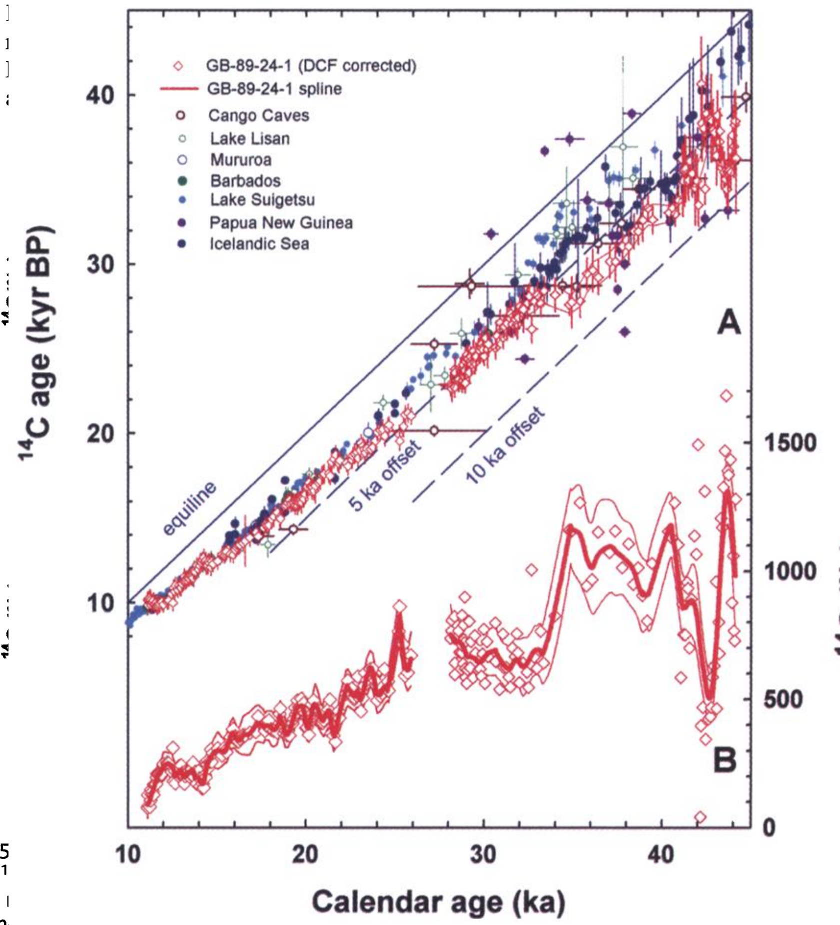

Fig. 4. Comparison between GB-89-24-1 $\Delta^{14}C$, 45 confidence intervals), and predicted atmospheric Δ^1 model experiments (*54*). (**A**) Global ^{14}C production intensity only, with the SINT200 stacked-geomagn invariant modern balanced carbon cycle with a steady state assumption was specified for this simulation (*54*). After 72 ka of run time, ^{14}C and ^{12}C levels returned to modern values in all model reservoirs. However, predicted atmospheric ^{14}C levels were substantially lower than observed in GB-89-24-1 during the last glacial period, and no major excursions were observed in the model output. (**B**) As in (A), except that both geomagnetic and solar magnetic fields were arbitrarily set to zero field strength between 44.5 and 43.8 ka. This experiment produced an atmospheric $\Delta^{14}C$ excursion of about 50% of the magnitude of the ~44-ka spike observed in GB-89-24-1 but failed to produce the generally high levels observed between 44 and 33 ka. (**C**) As in (B), except that the carbonate sedimentation rate was reduced to 0.24 Pg of C year^{-1} until 25 ka and then was gradually increased, reaching modern levels (2.0 Pg of C year^{-1}) at 11 ka. This model produced features similar to those observed in GB-89-24-1, but the ~44-ka excursion was smaller in amplitude than that observed in GB-89-24-1. (**D**) As in (C), except that the rate of thermohaline overturn was two-thirds of the modern level until 35 ka, when it was gradually increased, reaching modern levels at 11 ka. This model produced an even better match to the general features of the stalagmite record, and the ~44-ka excursion was of similar amplitude to that in GB-89-24-1. These models demonstrate that in addition to changes in ^{14}C production rate, changes in the carbon cycle are necessary to reproduce the GB-89-24-1 record of atmospheric ^{14}C.

carbon cycle. This is because enhancement of ^{14}C production to this level for such a duration increases the ^{14}C concentration of the deep ocean reservoirs. These reservoirs have long residence times, and the return flux of ^{14}C from the ocean is sufficient to keep atmospheric $\Delta^{14}C$ elevated for an extended period. Thus, invoking an increase in GCR to explain the 44-ka spike would still seem to require the carbon cycle to have operated substantially differently than today.

We suggest that substantially different modes of the carbon cycle must be invoked to explain the high levels of atmospheric ^{14}C observed in our stalagmite record for the last glacial period. Such high levels of atmospheric ^{14}C can be achieved by modulating carbonate sedimentation and dissolution rates or by changing the strength and/or depth of thermohaline circulation (THC). Both mechanisms result in increased storage of ^{14}C in the atmosphere when sedimentation rate is low or THC is sluggish or shallow. Figure 4C shows results from a model simulation identical to that presented in Fig. 4B, except that carbonate sedimentation rate was reduced to 0.24 Pg of C year^{-1} (*60*) until 25 ka and then gradually increased to modern levels (2.0 Pg of C year^{-1}) by the end of the last deglaciation (~11 ka). Equivalent and opposite changes in the dissolution flux from ancient (^{14}C depleted) sediments were also made to maintain a constant "active" carbon cycle size. This model simulation produces a first-order trend similar to the GB-89-24-1 record and exhibits increased sensitivity to rapid secular changes in geomagnetic field; however, it does not produce a ^{14}C excursion as

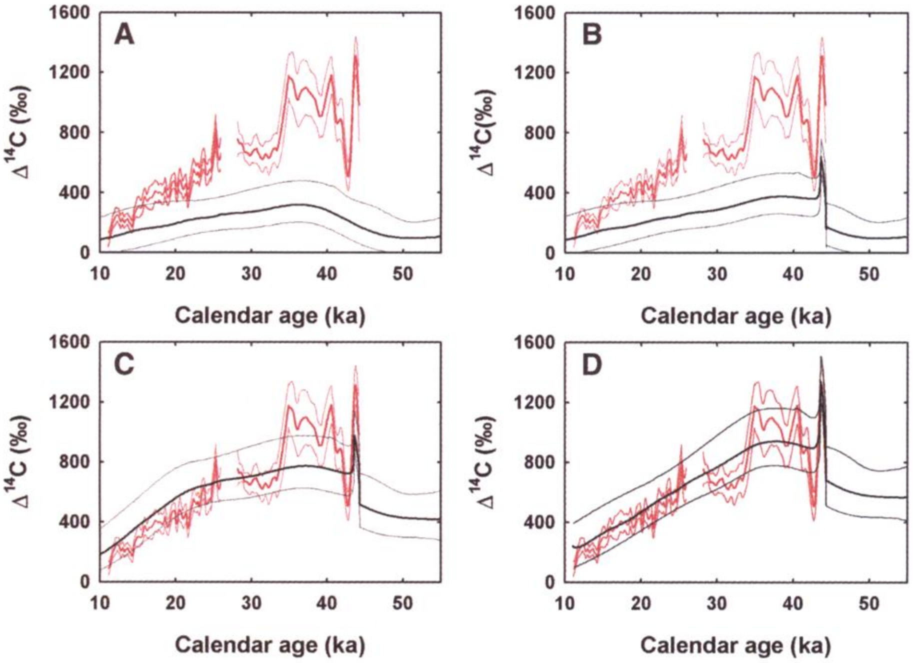

To produce the largest ^{14}C excursion (~44 ka) observed in our stalagmite record would require a nearly stagnant ocean, however, in which thermohaline circulation was completely shut down. In one such scenario, placing a barrier to exchange at midthermocline depth in the ocean (~350 m) makes it possible to increase atmospheric $\Delta^{14}C$ at a rate of ~2‰ year^{-1} for the SINT200 geomagnetic conditions present at ~44 ka. A ^{14}C spike as large as the ~44-ka excursion can then be produced in the requisite period, and reconnection with deep ocean circulation would rapidly drop atmospheric ^{14}C to previous levels, as observed. The other excursions observed in our stalagmite record could also be produced in this manner. Although a stagnant ocean is certainly an extreme scenario, it is nevertheless interesting to speculate about possible breakdowns of THC as part of the explanation for the ^{14}C excursions because of the similar timing between the ~44-ka ^{14}C spike and Heinrich event H5 (*61*). Comparable but smaller ^{14}C excursions appear to occur in our record at roughly the same time as H4, H3, H2, and H1. Because Heinrich events may in some cases substantially reduce surface ocean salinity in the high-latitude oceans, a potential mechanism exists for modulating atmospheric $\Delta^{14}C$ by varying THC (*7*, *59*, *61*).

Extreme reduction of THC cannot, however, be invoked as a mechanism to produce the excursions in cosmogenic isotopes ^{10}Be and ^{36}Cl observed in sediments and ice cores between 30 and 45 ka (*37–39*, *62*). Excursions in the flux of these isotopes require substantially reduced solar or geomagnetic modulation of GCR or changes in primary GCR intensity. Because these ^{10}Be and ^{36}Cl excursions are due in part to the same phenomena that affect atmospheric ^{14}C changes

References and Notes

1. M. Stuiver *et al.*, *Radiocarbon* **40**, 1041 (1998).
2. $\Delta^{14}C$ as used here is defined by the equation $\Delta^{14}C = 1000(Fe^{\lambda t} - 1)$ ‰, where F is the reservoir-corrected Fraction Modern, λ is the true ^{14}C decay constant, and t is the calendar age.
3. E. Bard *et al.*, *Nature* **382**, 241 (1996).
4. E. Bard, M. Arnold, B. Hamelin, N. Tisnerat-Laborde, G. Cabioch, *Radiocarbon* **40**, 1095 (1998).
5. G. S. Burr *et al.*, *Radiocarbon* **40**, 1093 (1998).
6. R. L. Edwards *et al.*, *Science* **260**, 962 (1993).
7. Y. Yokoyama, T. M. Esat, K. Lambeck, L. K. Fifield, *Radiocarbon* **42**, 383 (2000).
8. A. Schramm, M. Stein, S. L. Goldstein, *Earth Planet. Sci. Lett.* **175**, 27 (2000).
9. S. Björck *et al.*, *Science* **274**, 1155 (1996).
10. T. Goslar, M. Arnold, N. Tisnerat-Laborde, J. Czernik, K. Wiecedilckowski, *Nature* **403**, 877 (2000).
11. K. A. Hughen *et al.*, *Nature* **391**, 65 (1998).
12. K. A. Hughen, J. R. Southon, S. J. Lehman, J. T. Overpeck, *Science* **290**, 1951 (2000).
13. H. Kitagawa, J. van der Plicht, *Science* **279**, 1187 (1998).
14. A. H. L. Voelker *et al.*, *Radiocarbon* **40**, 517 (1998).
15. J. Beer, G. M. Raisbeck, F. Yiou, in *The Sun in Time*, C. P. Sonett, M. S. Giampapa, M. S. Matthews, Eds. (Univ. of Arizona Press, Tucson, AZ, 1991), pp. 343–359.
16. E. Bard, *Geochim. Cosmochim. Acta* **62**, 2035 (1998).
17. M. Frank, *Earth Planet. Sci. Lett.* **149**, 121 (1997).
18. R. Muscheler, J. Beer, G. Wagner, R. Finkel, *Nature* **408**, 567 (2000).
19. J. C. Vogel, J. Kronfeld, *Radiocarbon* **39**, 27 (1997).
20. GB-89-24-1, collected in 1989 from −14.4 m in Sagittarius, Zodiac Cavern 6, eastern Grand Bahama, is composed of dense, macrocrystalline calcite and shows no sign of postdepositional alteration. The longitudinal growth axis is 620 mm.
21. H. Cheng *et al.*, *Chem. Geol.* **169**, 17 (2000).
22. R. L. Edwards, J. H. Chen, G. J. Wasserburg, *Earth Planet Sci. Lett.* **80**, 241 (1987).
23. Of 81 U and Th measurements, 9 were duplicates split before chemical separation (either as powdered separates or chips from the same growth layer) and 5 were replicate dissolved and spiked samples put through chemistry separately.
24. Subsamples for ^{230}Th were drilled (<4-mm depth) at an angle oblique to the plane of the polished surface and parallel with growth layering. Time spans sampled for ^{230}Th analysis were intended to be similar to achievable age precision. Age estimates correspond to the midpoint along the longitudinal growth axis of each subsample.
25. K. R. Ludwig, D. M. Titterington, *Geochim. Cosmochim. Acta* **54**, 5031 (1994).
26. A. Kaufman [*Geochim. Cosmochim. Acta* **57**, 2303 (1993)] suggests using a worldwide $^{230}Th/^{232}Th$ activity value of 1.7 ± 0.7 in the absence of independent data.
27. R. L. Edwards, H. Cheng, M. T. Murrell, S. J. Goldstein, *Science* **276**, 782 (1997).
28. D. A. Pickett, M. T. Murrell, R. W. Williams, *Anal. Chem.* **66**, 1044 (1994).
29. Accelerator mass-spectrometric (AMS) ^{14}C analyses require a minimum of 1 mg of C (or 8.33 mg of $CaCO_3$) to obtain a 1σ precision of ~80 years at 12,000 yr B.P. and 1200 years at 40,000 yr B.P. Low U concentrations (59.1 to 228.1 ng g^{-1}) demanded calcite samples >0.5 g to obtain similar precision for ^{230}Th ages. Subsamples for ^{230}Th were drilled (<4 mm depth) at an angle oblique to the plane of the polished surface and parallel with growth layering. Time spans sampled for ^{230}Th analysis were intended to be similar to achievable age precision. Age estimates correspond to the midpoint along the longitudinal growth axis of each subsample.
30. P. J. Green, B. J. Silverman, *Nonparametric Regression and Generalized Linear Models* (Chapman & Hall, London, 1994).
31. G. W. Burr, R. L. Edwards, D. J. Donahue, E. R. M. Druffel, F. W. Taylor, *Radiocarbon* **34**, 611 (1992).
32. E. Bard, *Paleoceanography* **3**, 635 (1988).
33. E. Bard *et al.*, *Earth Planet Sci. Lett.* **126**, 275 (1994).
34. D. Genty, M. Massault, *Radiocarbon* **39**, 33 (1997).
35. D. Genty *et al.*, *Radiocarbon* **41**, 251 (1999).
36. R. B. Alley *et al.*, *J. Geophys. Res.* **102**, 26367 (1997).
37. G. M. Raisbeck *et al.*, *Nature* **292**, 825 (1981).
38. S. Baumgartner *et al.*, *Science* **279**, 1330 (1998).
39. F. Yiou *et al.*, *J. Geophys. Res.* **102**, 26783 (1997).
40. L. R. McHargue, P. Damon, D. J. Donahue, *Geophys. Res. Lett.* **22**, 659 (1995).
41. E. Bard, B. Hamelin, R. Fairbanks, A. Zindler, *Nature* **345**, 405 (1990).
42. J. Masarik, J. Beer, *J. Geophys. Res.* **104**, 12,099 (1999).
43. D. Lal, in *Solar-Terrestrial Relationships*, G. C. Castagnoli, D. Lal, Eds. (Soc. Italiana di Fisica-Bologna-Itala, Bologna, Italy, 1988), pp. 216–233.
44. ______, B. Peters, in *Progress in Elementary Particle and Cosmic Ray Physics*, J. G. Wilson, S. A. Wouthuysen, Eds. (North-Holland, Amsterdam, 1962), pp. 1–74.
45. E. T. Sundquist, W. S. Broecker, Eds., *The Carbon Cycle and Atmospheric CO_2: Natural Variations Archean to Present*, vol. 32 of Geophysical Monograph Series (American Geophysical Union, Washington, DC, 1985).
46. R. Reedy, in *Solar Particle Events and Their Radiation Threats, Conference on the High Energy Radiation Background in Space, Snowmass, CO* (IEEE Nuclear

and Plasma Sciences Society and the Institute of Electrical and Electronic Engineers, location, 1998), pp. 317–323.
47. E. N. Parker, in *Cosmic Winds and the Heliosphere*, J. R. Jokipii, C. P. Sonett, M. S. Giampapa, Eds. (Univ. of Arizona Press, Tucson, AZ, 1997), pp. 3–27.
48. E. J. Smith, in *The Sun in Time*, C. P. Sonett, M. S. Giampapa, M. S. Matthews, Eds. (Univ. of Arizona Press, Tucson, AZ, 1991), pp. 175–201.
49. P. Damon, C. P. Sonnet, in *The Sun in Time*, C. P. Sonnet, M. S. Giampapa, M. S. Matthews, Eds. (Univ. of Arizona Press, Tucson, AZ, 1991), pp. 360–388.
50. M. Stuiver, *J. Geophys. Res.* **66**, 273 (1961).
51. J. C. Houtermans, thesis, University of Bern, Bern, Switzerland (1971).
52. H. E. Suess, *Radiocarbon* **22**, 200 (1980).
53. K. O'Brien, A. D. L. Z. Lerner, M. A. Shea, D. F. Smart, in *The Sun in Time*, C. P. Sonnet, M. S. Giampapa, M. S. Matthews, Eds. (Univ. of Arizona Press, Tucson, AZ, 1991), pp. 317–343.
54. A 13-box carbon cycle model was used that included reservoirs for the atmosphere, terrestrial biosphere, soils, ocean sediments, and a 9-box ocean. Reservoir size and fluxes were brought to an initial balanced state in which both ^{12}C and ^{14}C concentrations reflected the modern prebomb pulse abundances (*45*, *55*, *56*). A globally averaged modern ^{14}C production rate of 2.03 atoms cm^{-2} s^{-1} was used (*42*), although this value is probably uncertain to about ±10% (*63*). The terrestrial magnetic field intensity dependence used (*42*) assumes a solar modulation parameter of $\phi = 550$ equal to an average value for the period 1953–95, whereas the SINT200 (*57*) stacked paleomagnetic record was used as the record of terrestrial magnetic field intensity. The total active carbon reservoir size was set at 54,600 Pg of C, as required by a steady state ^{14}C production rate of 2.03 atoms cm^{-2} s^{-1} and the known modern ^{14}C activities in the various reservoirs (*55*). We define the active carbon reservoir as that carbon that may exchange with the atmosphere on 50-ka time scales. Because the production rate could only have been greater in the past 50 ka (because we are now at a geomagnetic maximum), the minimum size of the active carbon cycle is determined in the following way: If $(\partial N/\partial t)$ global = 2.03 atoms cm^{-2} s^{-1} × area of Earth, then the global ^{14}C inventory is given by $(\partial N/\partial t)$ global/λ_{14C} (global), and the inventory of ^{12}C is given by ^{14}C(global)/($^{14}C/^{12}C$)average = ^{12}C(active carbon cycle). Thus, ^{12}C(active carbon cycle) = 54,600 Pg of C. Because there are only 39,400 Pg of C (*45*) in the ocean + atmosphere + biosphere + active terrestrial soils, this means there are additionally about 15,200 Pg of C contained in other parts of the active carbon cycle. The only element of the active carbon cycle large enough to contain this amount of carbon is ocean carbonate sediments. If these sediments are formed in the ocean mixed layer, then the initial ($^{14}C/^{12}C$) must be the same as that of the mixed layer (i.e., FM = 0.85). This implies that at steady state the flux of carbon to this sedimentary sink must be on average 1.85 Pg of C $year^{-1}$.
55. W. S. Broecker, T.-H. Peng, *Tracers in the Sea* (Lamont-Doherty Geological Observatory, Palisades, NY, 1982).
56. G. Munhoven, thesis, Université de Liége, Liége, Belgium (1997).
57. Y. Guyodo, J.-P. Valet, *Earth Planet. Sci. Lett.* **143**, 23 (1996).
58. C. Laj, C. Kissel, A. Mazaud, J. E. T. Channel, J. Beer, *Philos. Trans. R. Soc. London* **358**, 1009 (2000).
59. C. Kissel *et al.*, *Earth Planet. Sci. Lett.* **171**, 489 (1999).
60. Most estimates of carbonate sedimentation rates for the modern world range between 0.24 and 2.0 Pg of C $year^{-1}$.
61. H. Heinrich, *Quat. Res.* **29**, 143 (1988).
62. P. E. Damon, R. E. Sternberg, *Radiocarbon* **31**, 697 (1989).
63. R. C. Finkel, K. Nishiizumi, *J. Geophys. Res.* **102**, 26699 (1997).
64. This paper is dedicated to the memory of R. Palmer and R. Parker, who died in separate diving incidents in 1997. We are extremely grateful to both of them for their invaluable contributions to exploration and fieldwork in the Blue Holes of the Bahamas.

17 October 2000; accepted 24 April 2001
Published online 11 May 2001;
10.1126/science.1056649
Include this information when citing this paper.

REPORTS

Ultrafast Manipulation of Electron Spin Coherence

J. A. Gupta,[1] R. Knobel,[2] N. Samarth,[2] D. D. Awschalom[1]*

A technique is developed with the potential for coherent all-optical control over electron spins in semiconductors on femtosecond time scales. The experiments show that optical "tipping" pulses can enact substantial rotations of electron spins through a mechanism dependent on the optical Stark effect. These rotations were measured as changes in the amplitude of spin precession after optical excitation in a transverse magnetic field and approach $\pi/2$ radians. A prototype sequence of two tipping pulses indicates that the rotation is reversible, a result that establishes the coherent nature of the tipping process.

Multiple pulse sequences in time-domain nuclear magnetic resonance and electron spin resonance (ESR) experiments are widely used to study spin-spin interactions and spin dephasing in inhomogeneous magnetic environments (*1*). A canonical sequence consists of a $\pi/2$ pulse to generate a nonequilibrium transverse spin polarization followed by a π-pulse that may enact a rephasing ("spin echo") of transverse spin if inhomogeneous broadening dominates the ensemble spin dynamics (*2*). Current technology limits the number of systems to which pulsed-ESR experiments can be applied because the minimum achievable pulse length of ~10 ns should be much smaller than the spin coherence time (*1*). To apply pulse sequences to study conduction-band electron spin dynamics in a variety of semiconductors where spin lifetimes can vary from ~3 ps (*3*) to ~130 ns (*4*), a complementary ESR technique capable of much shorter pulse widths is desirable. Application of spin echo sequences might be of particular interest in semiconductor quantum dots, where inhomogeneous broadening can limit spin lifetimes (*5*). Such a technique could also be useful for spin-based implementations of quantum computing in solid-state systems (*6*), where it is necessary to perform many operations ($>10^4$) on a quantum bit within the coherence time to realize full computation with error correction (*7*). The ability to perform spin operations on femtosecond time scales would satisfy this need in a number of semiconductor systems and may be applicable to single quantum bits using optical probes with high spatial resolution.

Here we present time-resolved Faraday rotation experiments that extend a technique first applied in atomic sodium (*8*) to semiconductor nanostructures by using ultrafast laser pulses to produce coherent rotations of electron spins (*9*). In our experiments, a pump pulse optically excites spin-polarized electrons that precess about a static magnetic field. A second below–band gap "tipping" pulse produces an additional effective magnetic field that can reach 20 T through the optical Stark effect (*10*). Effective field strengths are calculated from measurements of Stark shifts and depend on the pulse intensity, polarization, and energy. This field is used to coherently rotate electron spins by angles that approach $\pi/2$, as monitored through the Faraday rotation imparted to a probe pulse. A sequence of two tipping pulses suggests that spin coherence is preserved during the tipping process. Because the tipping pulses additionally excite a small number of real carriers, a variety of checks were performed to identify resultant background contributions. Although the tipping effects can be qualitatively interpreted as rotations about a light-induced effective field, quantitative comparisons of the tipping angle from Faraday rotation data with that expected from measured Stark shifts reveal a significant discrepancy.

Samples were chosen that illustrate a variety

[1]Department of Physics, University of California, Santa Barbara, CA 93106, USA. [2]Department of Physics, The Pennsylvania State University, University Park, PA 16802, USA.

*To whom correspondence should be addressed. E-mail: awsch@physics.ucsb.edu